How to Cite:
Karape, S. M., Sirsat, D. M., Pakhare, K. S., Jadhav, S. S., & Sankpal, S. T. (2022). Synthesis and characterization of arrested precipitation assembled Cu2Se thin films. *International Journal of Health Sciences*, *6*(S6), 764–773.
https://doi.org/10.53730/ijhs.v6nS6.9674

Synthesis and characterization of arrested precipitation assembled Cu2Se thin films

S. M. Karape*
Assistant Professor Anandibai Raorane Arts, Commerce and Science College, Vaibhavwadi, Maharashtra, India

D. M. Sirsat
Assistant Professor, Anandibai Raorane Arts, Commerce and Science College, Vaibhavwadi, Maharashtra, India

K. S. Pakhare
Assistant Professor, Anandibai Raorane Arts, Commerce and Science College, Vaibhavwadi, Maharashtra, India

S. S. Jadhav
Assistant Professor, Materials Research Laboratory, P. G. Department of Chemistry, Balwant College Vita, Maharashtra, India

S. T. Sankpal
Assistant Professor, Dept. of Chemistry, Athalye Sapre Pitre College Devrukh, Ratnagiri, Maharashtra, India

***Abstract*---**Nanostructured thin films of copper selenide (Cu2Se) deposited by arrested precipitation technique (APT) with controlled release of ions at suitable pH=10.5. The deposited Cu2Se films were characterized for optical, structural, and morphological properties. Optical absorption study indicates that the band gap energy (2.26 eV) of material and shows visible radiation absorption. XRD shoe that APT is a favorable technique for the synthesis of pure nanocrystalline Cu2Se thin films with monoclinic crystal structure. An electrochemical impedance spectroscopy analysis confirms the charge transfer resistance. X-ray photoelectron spectroscopy reveals stoichiometry at valance state of Cu2Se.

***Keywords*---**arrested precipitation technique, thin films, copper selenide, optical properties.

Introduction

Nanostructured thin film solar cells are a favorable and perhaps emergent technology these days [1]. Stoichiometric nanostructured inorganic semiconductor coatings will be superior options for engineering solar cells and limiting the depletion of nonrenewable energy supplies such as fossil fuels, natural gas, and coal oils [2]. Copper-containing chalcogenides compound semiconductors have so concentrated on ultra-thin absorber layers [3], counter electrodes such as Cu_2S [4] and CuSe [5]. Metal chalcogenide thin films are easy to deposit on substrates like glass and plastic, making them ideal for solar building integration as optoelectronic devices. The IB-VIA and II-VIA group chalcogenides are becoming more attractive due to their strong absorption coefficient in visible light and electron-hole separations during solar cell operation [6]. Copper selenide (Cu_2Se, 2.2 eV) [7] is semiconducting and visible radiation active [8-13]. However, they lack generality or need complex equipment, and they are problematic due to the use of hazardous reducing agents, surfactants, solvents, and high temperatures in the synthesis of copper chalcogenide compounds [10]. As a result, solution-processed synthesis utilising the APT approach is easy and cost-effective [11], with structural, compositional, and opto-electrical characteristics equivalent to those of other advanced deposition methods [12].

We used triethanolamine (TEA) as a polydentate ligand in this study, which forms a complex with copper metal ions to prevent bulk precipitation. The goal of this report's innovation is to improve the growth mechanism conditions, particularly the reduction of copper metal ions owing to mild reducing agents (Na_2SO_3), such that Cu_2Se thin films have a homogeneous, highly adherent nanogranular surface shape at room temperature. APT is a chemosynthesis of ternary nanoalloys using a hybrid chemical bath deposition approach in tandem with the controlled chemical growth process (CCGP) [11]. In inorganic metal chalcogenide coating thin films, smaller crystallites serve as nutrition to the directed bigger developing crystallites [14, 15]. Although the possible growth and response mechanisms for Cu_2Se thin film production were briefly explored.

Experimental Details

Materials and method

Without additional purification, all of the compounds employed were analytical reagent (AR) grade. Precursors included copper sulphate pentahydrate ($CuSO_4$, $5H_2O$), selenium metal powder, sodium sulfite (Na_2SO_3), ammonia solution (NH_3), and triethanolamine ($N(CH_2CH_2OH)_3$). We created a sulfide/polysulfide redox mediator with sodium sulphide (Na_2S), sodium hydroxide pellets (NaOH) , and sulphur powder . The substrates were cleaned using a chromic acid solution heated to 500°C for 5 minutes before being ultrasonically cleaned with a combination of isopropanol and demonised water. Cu_2Se thin films were produced on naked glass substrates using a simple APT chemosynthesis method.

Synthesis of Cu_2Se thin films

Simple chemical processes were the focus of a recent synthetic route. To create the clear translucent solution, 0.05 M copper sulphate solutions were employed to form a complex with triethanolamine (TEA) as a polydentate ligand. At alkaline pH=10.5, the Cu^{2+}–$(TEA)_2$ complex interacts with the Se^{2-} chalcogen ions, releasing slowly by dissociation of Sodium selenosulfite (Na_2SeSO_3). Refluxing selenium metal powder with anhydrous sodium sulfite (Na2SO3) at 70 °C for 10 hours yielded Na2SeSO3. The nucleation and Ostwald's ripening mechanisms were used to deposit Cu_2Se thin films. Different preparative factors such as ligand concentration, Cu^{2+} precursor concentration, pH, deposition period, single-solution phase, and bath temperature are mostly responsible for these mechanisms. As a result, all of these parameters were optimised at the thin film deposition initiative stage. The precursor concentration of 0.05 M Cu^{2+} was kept constant, as was the deposition duration at ambient temperature (RPM). A surface profiler was used to measure the thickness of the Cu_2Se films after they were formed. After the depositions are completed, the substrate peels away from the overgrowth surface, with no increase in film thickness. All of the deposited thin films were homogenous, highly adhering translucent blackish tinted at the terminal development phase.

Characterizations

A UV-Vis-NIR spectrophotometer was used to capture optical absorption spectra (Shimadzu, UV-1800). An X-ray diffractometer (Bruker AXS, D8) was used to validate structural characteristics using Cu Kα (λ= 1.5418 Aº) radiation for 2θ from 20º to 80º. Field-emission scanning electron microscopy (FE-SEM) and X-ray photoelectron spectroscopy (XPS, Thermo Scientific, Multilab-2000) with a multi-channel detector that can withstand high photon energies from 0.1 to 3.0 keV were used to demonstrate the surface morphology and elemental composition of the deposited thin films. The auto lab PGSTAT 100 FRA 32 was used to conduct the EIS.

Results and Discussion

Thin films formation and its growth mechanism

It may be feasible to analyze attributes of deposited material with chosen morphology and crystalinity in order to determine how shape evolution processes are predictable. Cu^{2+} metal ions are complexed utilizing complexion (TEA) and released slowly at the optimal precursor concentration, temperature, and pH in the current process. By raising the concentration of OH^- ions and the proportionate rise in chalcogen ions Se^{2-} releasing ability in the reaction solution, aqueous NH_3 is employed to adjust the pH [11]. However, when the temperature rises, the rate of metal ions released rises, and the reaction accelerates, resulting in bulk precipitation rather than the desired quality thin film production. As a result, we must first improve depositions at room temperature (300 K), Cu^{2+} precursor concentrations of 0.05 M, and pH of 10.5. Cu_2Se thin films of exceptional quality and uniformity were synthesized. APT approaches are based on nucleation and the Ostwald ripening mechanism. When the ionic product (Kp)

of the metal ions exceeds the solubility product (Ksp), thin films are formed. Following the ion-by-ion condensation of metal ions onto the substrate surface, the nucleation process begins [11]. A delayed reaction rate produces good stochastic compositions with high-quality and adhesive thin films in general [16]. As a result, as compared to traditional chemical bath methods, the hybrid created arrested precipitation methodology is more effective.

Reaction mechanism of Cu_2Se thin film formation

Solution of Cu^{2+} ions are complexes with Triethanolamine (TEA) as complexion (1)

$$CuSO_4 5H_2O + 2(CH_2CH_2OH)_3N \Rightarrow [Cu((CH_2CH_2OH)_3N)_2]SO_4 + 5H_2O \quad \ldots\ldots (1)$$

With addition of basic solution of 30 % liquor NH_3, the Cu^{2+} ions released due to the dissociation of metal complex bonds at alkaline pH = 10.5 as explained in reaction (2)

$$[Cu^{2+} - (TEA)_2]SO_4 + 2NH_4OH \xrightarrow{RT} \Rightarrow Cu^{2+} + 2[N(CH_2CH_2OH)_3] + (NH_4)_2SO_4 + 2OH^-$$

.....(2)

Sodium selenosulfite dissociates into sodium sulfite and highly active HSe^- species at the same pH and ambient temperature. By absorbing protons in alkaline media reactions (3), this highly active species swiftly transforms into reactive Se^{2-} ions (4) [17]

$$Na_2SeSO_3 + H^+ \Rightarrow Na_2SO_3 + HSe^-$$
.....(3)
$$HSe^- + OH- \Rightarrow Se^{2-} + H_2O$$
.....(4)

The sodium sulfites released are actions as mild reducing agents and forms the sodium sulfate is shown in eqn. (5) [18].

$$Na_2SO_3 + H_2O \Rightarrow Na_2SO_4 + 2H^+ + 2e^-$$
……(5)
The ionic product of the Cu^{2+} and Se^{2-} ions surpasses the solubility product in the reaction bath during the creation of Cu_2Se thin films, resulting in a gradual ion-by-ion condensation of the metal and chalcogen ions according to the Ostwald ripening law. The moderate reducing agents Na_2SO_3 make the condensed Cu^{2+} metal ions more reactive and easy to reduce, as illustrated in reactions (6) [18].

$$2Cu^{2+} + 2e^- \Rightarrow 2Cu^+$$
…….(6)

Finally the free anions combined with cations to form Cu_2Se are summarized in below as (7)

$$2Cu^{+} + Se^{2-} \Rightarrow Cu_2Se \quad \ldots\ldots(7)$$

Optical studies

The absorption spectra of UV-Vis-NIR (ultraviolet-visible-near infrared) in the wavelength range 300–900 nm were shown in Fig. 1. The Cu_2Se thin films' optical absorption spectra were obtained and clearly demonstrated that the highest visible light absorption occurs between 400 and 550 nm. All of the samples had an absorption coefficient on the order of 105 cm-1. The optical band gap energy may be calculated using electron excitation from the valance band to the conduction band. The term "optical data" refers to the use of the equation (8)

$$\alpha = \frac{A(h\vartheta - E_g)^n}{h\vartheta} \quad \ldots\ldots(8)$$

When A denoted as a transition probability parameter, h denoted as the Planck constant, Eg denoted as the material's optical band gap energy, and the exponent (n) is dependent on the kind of transition. 1/2, 2, 3/2, and 3 are the values of (n) for direct allowed, indirect allowed, direct prohibited, and indirect forbidden transitions, respectively. The optical band gap energy values of Cu_2Se thin films were calculated using the graph of $(\alpha h\nu)^2$ versus $(h\nu)$ ((eV/cm)2 vs (eV)), as shown in the inset of Fig. 1.

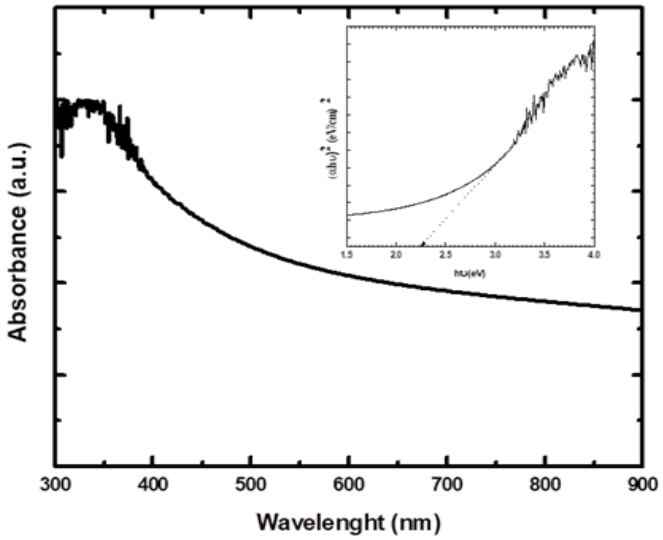

Fig. 1. Optical absorption spectra of the Cu_2Se thin films, inset is plot of $(\alpha h\vartheta)^2$ vs $(h\vartheta)$.

Structural studies

X-ray diffraction measurements in the range 2θ of 20º to 70º were used to record the crystal structure analysis of the sample. The Cu_2Se thin film's XRD pattern is shown in Figure 2. The Cu_2Se thin films are nanocrystalline by nature, as evidenced by the XRD pattern, which exhibits both wide and strong peaks [19].

The primary diffraction peaks were concentrated at 2θ = 27.44º, 43.82º, 51.34º, 51.81º, and 54.44°, which corresponded to the monoclinic crystal system's (111), (220), (311), (311), and (222) planes. Peaks emerge at same sites in a typical XRD examination of Cu_2Se thin films, with changes to the intensity and expansion of the diffraction peaks, indicating the development of pure phase materials with increased crystalinity. Some of the minor intensity peaks demonstrate the amorphous character of the films due to the presence of glass beads in the materials. Furthermore, no further peaks are seen, indicating that the substance is in its pure phase. Strain or micro-strain might explain the observed widening of the diffraction peaks. The crystallite size was also determined using the Debye Scherer formula equation (9) [19].

$$D = \frac{0.9\lambda}{\beta \cos\theta} \qquad \text{.....(9)}$$

where D denotes the crystallite size, λ=1.5406 is the X-ray wavelength, FWHM denotes the radians is the full-width-at-half-maximum (FWHM), and θ denotes the Bragg's angle and the crystallite size calculated is 24 nm.

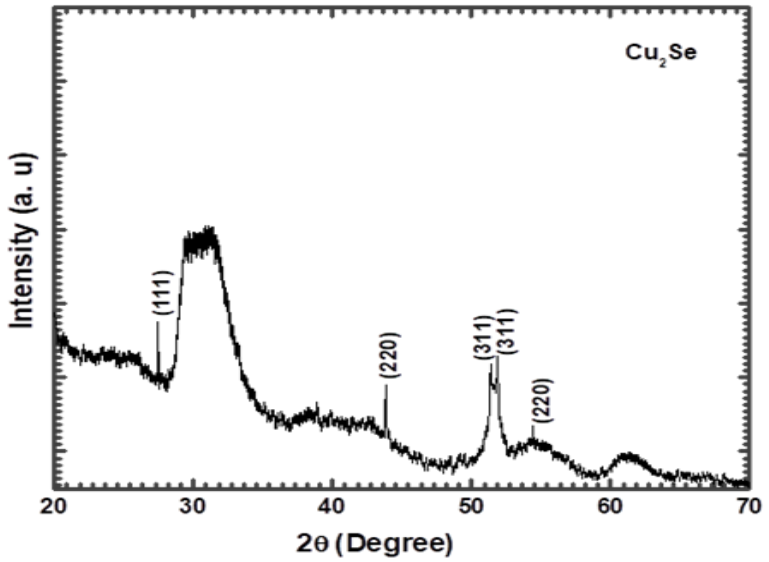

Figure 2. XRD pattern of the Cu_2Se thin film.

Electrochemical impedance spectroscopy (EIS)

The Cu_2Se thin film's PEC kinetics were investigated using EIS. EIS measurements were carried out in the dark using a 0.2 M polysulfide mediator and a 0.5 V forward bias voltage. The ac frequency range that was measured was 0.1 Hz to 1000 Hz. The Nyquist plot of Cu_2Se thin film is shown in Figure 3. The solution resistance (Rs= 25 Ω cm^{-2}) R1 is the charge transfer resistance between the Pt-FTO counter/electrolyte interface, whereas R2 is the charge transfer resistance due to photo-excited electron hole recombination at Cu_2Se/mediator.

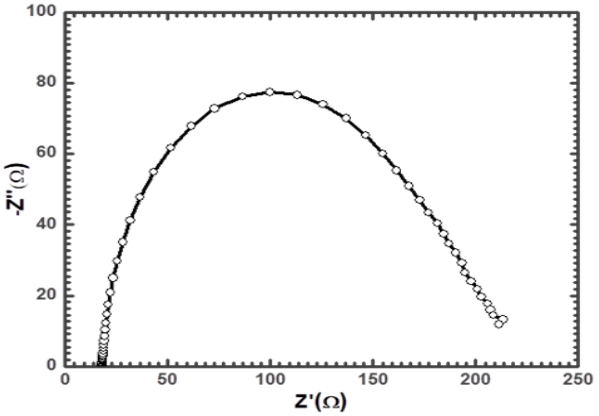

Figure 3. Nyquist plot of Cu_2Se thin film.

Morphological Studies

The surface morphology of Cu_2Se thin films may be seen using field-emission scanning electron microscopy (FE-SEM). FE-SEM micrographs of Cu_2Se thin films at low and high magnification are shown in Fig. 4. FE-SEM micrographs revealed that nanoflakes were evenly distributed over the whole surface. At lower precursor concentrations, a beaded nanoflakes-like morphology was observed. Cu_2Se materials with tiny grain sizes develop at a lower concentration and are distributed throughout the whole substrate surface. The grain size of these nanoflakes-like materials is less than ~40 nm.

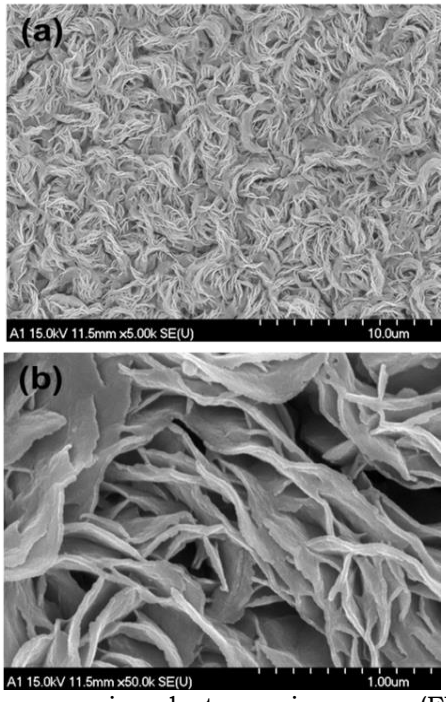

Figure 4. Field-emission scanning electron microscopy (FE-SEM) (a) low and (b) high magnification images of Cu_2Se

Compositional Analysis

In order to check the surface elemental composition of the Cu_2Se thin film. The XPS survey and high resolution core level spectrum demonstrated in Fig. 5. The two distinct peaks confirm the presence of Copper and Selenium elements respectively. Additionally, elements valance state and the existing form of the Cu_2Se thin film was investigated by XPS study as shown in Fig. 5 (a), peaks along with Carbon and Oxygen in the sample.

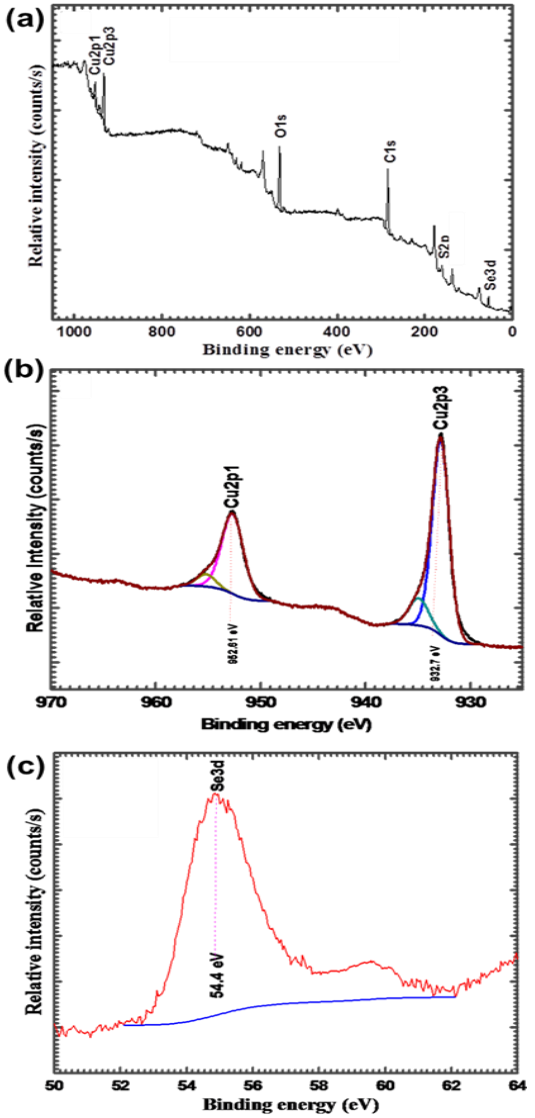

Figure 5. (a) XPS survey spectrum of Cu_2Se thin film, (b) high-resolution core level XPS spectrum of Cu, (c) high- resolution core level XPS spectrum of Se.

Copper's spectrum at its most fundamental level Cu2p peaks can be readily recognised in Fig.5 (b), with two peaks ascribed to Cu2p3/2 and Cu2p1/2 with

binding energies of 932.7 eV and 952.61 eV, respectively, indicating the existence of Cu^{+} in the sample. Cu2p3/2 and Cu2p1/2 were also assigned two peaks with binding energies of 932.7 eV and 952.61 eV, respectively, indicating the existence of Cu^{+} with a splitting energy of 19.91 eV [7] [20]. The presence of Se2-is verified by a significant peak at 54.4 eV ascribed to the Se3d transition in Fig. 5 (c). For the Cu^{+} and Se^{2-} states, the binding energies for Cu and Se are at their corresponding locations. It denotes the presence of Cu+ and Se^{2-}. It means that Cu^{+}, and Se^{2-} exists in the stochastic formula of deposited Cu_2Se thin film.

Conclusion

All of the above discussion and analysis indicate that nanoflakes Cu_2Se thin films were effectively created for the first time employing the single-solution phase arrested precipitation approach. Cu_2Se thin film has control over directed crystal formation due to vital function including TEA, the band gap energy 2.26 eV, according to opto-structural and morphological research. The crystalline nature of the sample is shown by the XRD pattern, which reveals a pure monoclinic crystal structure that governs the ion insertion kinetics leading to a charge transfer process. XPS confirms the stochastic Cu_2Se thin film at chemical valance state.

References

1. Chen G, Seo J, Yang C, Prasad PN (2013) Nanochemistry and nanomaterials for photovoltaics. ChemSoc Rev 42:8304–38.
2. Khot K V., Mali SS, Pawar NB, et al (2014) Development of nanocoral-like Cd(SSe) thin films using an arrested precipitation technique and their application. New J Chem 38:5964–5974.
3. Page M, Niitsoo O, Itzhaik Y, et al (2009) Copper sulfide as a light absorber in wet-chemical synthesized extremely thin absorber (ETA) solar cells. Energy Environ Sci 2:220–223.
4. Jun HK, Careem MA, Arof AK (2014) Performances of some low-cost counter electrode materials in CdS and CdSe quantum dot-sensitized solar cells. Nanoscale Res Lett 9:69–76.
5. Liu F, Zhu J, Hu L, et al (2015) Low-temperature, solution-deposited metal chalcogenide films as highly efficient counter electrodes for sensitized solar cells. J Mater Chem A 3:6315–6323.
6. Dilena E, Dorfs D, George C, et al (2012) Colloidal $Cu_{2-x}(S_ySe_{1-y})$ alloy nanocrystals with controllable crystal phase: synthesis, plasmonic properties, cation exchange and electrochemical lithiation. J Mater Chem 22:13023–13031.
7. Li D, Zheng Z, Lei Y, et al (2010) Design and growth of dendritic $Cu_{2-x}Se$ and bunchy CuSe hierarchical crystalline aggregations. CrystEngComm 12:1856–1861.
8. Sagade AA, Sharma R (2008) Copper sulphide (CuxS) as an ammonia gas sensor working at room temperature. Sensors Actuators, B Chem 133:135–143.
9. Murali KR, Xavier RJ (2009) Characteristics of brush electroplated copper selenide thin films. Chalcogenide Lett 6:683–687.
10. Zhang P, Gao L (2003) Copper sulfide flakes and nanodisks. J Mater Chem 13:2007–2010.

11. Patil AR, Patil VN, Bhosale PN, Deshmukh LP (2000) Study of bismuth sulphoselenide thin films: Growth from the solution and properties. Mater Chem Phys 65:266–274.
12. Dhondge AD, Gosavi SR, Gosavi NM (2015) Influence of Thickness on the Photosensing Properties of Chemically Synthesized Copper Sulfide Thin Films. world J Condens matter Phys 5:1–9.
13. Jadhav SS, Mali SS, Hong CK, et al (2018) Arrested precipitation assembly of nanosheets Cu_2ZnCd (S, Se)$_3$ thin film for solar cell performance: Novel skilful synthesis. Mater Lett.
14. Jadhav SS, Hong CK, Patil PS, et al (2016) Novel synthesis of efficient counter electrode by facile arrested precipitation technique. J Mater Sci Mater Electron 4:3812–3820.
15. Zhang H, Penn RL, Lin Z, Cölfen H (2014) Nanocrystal growth via oriented attachment. CrystEngComm 16:1407–1408.
16. [16] Patil SP, Mane RM, Kharade RR, Bhosale PN (2012) Novel synthetic route for quaternary MoBiGaSe 5 mixed metal chalcogenide (mmc) thin films. Dig J Nanomater biostructures 7:237–245.
17. Kumar, S. (2022). A quest for sustainium (sustainability Premium): review of sustainable bonds. Academy of Accounting and Financial Studies Journal, Vol. 26, no.2, pp. 1-18
18. Allugunti V.R (2022). A machine learning model for skin disease classification using convolution neural network. International Journal of Computing, Programming and Database Management 3(1), 141-147
19. Allugunti V.R (2022). Breast cancer detection based on thermographic images using machinelearning and deep learning algorithms. International Journal of Engineering in Computer Science 4(1), 49-56
20. Ghanwat VB, Mali SS, Mane RM, et al (2015) Thermoelectric properties of nanocrystalline Cu3SSe4 thin films deposited by a self-organized arrested
21. Mousavi-Kamazani M, Salavati-Niasari M, Sadeghinia M (2015) Facile hydrothermal synthesis, formation mechanism and solar cell application of $CuInS_2$ nanoparticles using novel starting reagents. Mater Lett 142:145–149.
22. Pawar NB, Mali SS, Kharade SD, et al (2014) Influence of vacuum annealing on the structural and photoelectrochemical properties of nanocrystalline MoBi2S5 thin films. Curr Appl Phys 14:508–515.
23. Wang J, Xue D, Guo Y, et al (2011) Bandgap Engineering of Monodispersed $Cu_{2-x}SySe_{1-y}$ Nanocrystals through Chalgen Ratio and Crystal Structure. J Am Chem Soc 18558–18561.
24. Rinartha, K., Suryasa, W., & Kartika, L. G. S. (2018). Comparative Analysis of String Similarity on Dynamic Query Suggestions. In *2018 Electrical Power, Electronics, Communications, Controls and Informatics Seminar (EECCIS)* (pp. 399-404). IEEE.
25. Suryasa, I. W., Rodríguez-Gámez, M., & Koldoris, T. (2021). Get vaccinated when it is your turn and follow the local guidelines. *International Journal of Health Sciences*, *5*(3), x-xv. https://doi.org/10.53730/ijhs.v5n3.2938